# NOVEL VECTOR BEAMFORMERS FOR EEG SOURCE IMAGING

*Hung V. Dang, Kwong T. Ng**

New Mexico State University
Department of Electrical and Computer Engineering
P.O. Box 30001/MSC 3-O
Las Cruces, NM 88003

*James K. Kroger*

New Mexico State University
Department of Psychology
P.O. Box 30001/MSC 3452
Las Cruces, NM 88003

## ABSTRACT

This paper introduces two novel vector beamforming algorithms, namely the Vector Weight Normalized and Vector Standardized Minimum Variance beamformers, for brain source localization and reconstruction. Our mathematical analysis shows that the Vector Weight Normalized Minimum Variance beamformer (V-WNMVB) is the true vector version of the Synthetic Aperture Magnetoencephalography (SAM). Our Monte-Carlo simulation results with fixed and rotated dipole sources show that the two new vector beamformers give better source localization errors than the existing ones, including SAM, linearly constrained minimum variance beamformer and vector Borgiotti-Kaplan beamformer. Finally, the multiple dipole source simulation studies show that the performance of V-WNMVB is as good as that of SAM, however, it does not require any assumption on the source orientation.

## 1. INTRODUCTION

The recorded EEG signals have been used to localize and to reconstruct the brain sources, typically represented as electric current dipoles, in various applications [1]. Numerous inverse source localization algorithms have been proposed in the past [1]. Each of them relies on its own assumptions and constraints to localize the sources. Among them are the beamforming techniques which have been explored as a possible way to improve the spatial accuracy of source imaging [18, 13, 14, 9, 2, 6]. A beamformer is basically a spatial filter that can be applied at any place in the brain. By suppressing the effects of sources at all other locations, a beamformer allows us to estimate a brain activity at a particular place from a segment of EEG signals.

There are two major types of beamformers: 1) scalar ones in which the dipole orientation is assumed to be fixed and estimated separately; 2) vector ones that estimate the three dipole components simultaneously. Major scalar beamformers proposed in the past include the scalar minimum variance beamformer (S-MVB) [8], the scalar weight normalized minimum variance beamformer (S-WNMVB), the scalar standardized minimum variance beamformer (S-SMVB) [8], and the synthetic aperture magnetoencephalography (SAM) [13]. As for vector beamformers, the most popular one is the vector minimum variance beamformer or linearly constrained minimum variance beamformer (LCMV) [18]. The unit-noise power vector beamformer or vector Borgiotti-Kaplan beamformer (V-BKB) was introduced for MEG applications in [15], where it was shown to give a better performance than LCMV.

The motivation of our work arises from the need of a better vector beamformer for source imaging applications. Here, we introduce two novel vector beamformers: vector weight normalized minimum variance beamformer (V-WNMVB) and vector standardized minimum variance beamformer (V-SMVB). We also derive the analytical expressions for all the beamformer metrics studied, including the output power and output SNR. Moreover, efficient algorithms for computing the tomographic maps of the two new beamformers and SAM are introduced, which would stabilize the calculation when the lead field matrix is not full rank.

## 2. METHODS

### 2.1. Conventional beamformers

The scalar beamformers assume the source orientation is fixed, and their weight and orientation vectors are estimated separately. The source moment $\widehat{\mathbf{d}}(\mathbf{r})$ for a dipole located at $\mathbf{r}\,(x, y, z)$ and oriented in the direction $\mathbf{v}$ is reconstructed from measured EEG signals $\mathbf{M}$ by $\widehat{\mathbf{d}}(\mathbf{r}) = \mathbf{w}^T(\mathbf{r})\mathbf{M}$, where $\mathbf{w}$ is the weight vector. As mentioned earlier, three major scalar beamformers are compared in this study, namely the scalar minimum variance beamformer (S-MVB), the scalar weight normalized minimum variance beamformer (S-WNMVB) and the scalar standardized minimum variance beamformer (S-SMVB) [8]. The weight vector is obtained as the solution to the optimization problem

$$minimize \quad \mathbf{w}^T\mathbf{R}\mathbf{w} \quad subject\ to \quad \mathbf{w}^T\mathbf{g} = \xi \qquad (1)$$

*The research was supported in part by the Los Alamos National Laboratory and Army High Performance Computing Research Center.

where $\mathbf{R}$ is the covariance matrix, $\mathbf{w}^T\mathbf{R}\mathbf{w}$ is the output power of a scalar beamformer, $\mathbf{g} = \mathbf{L}\mathbf{v}$ is the gain vector, and $\mathbf{L}$ is the lead field matrix. The Lagrange multiplier technique [18] can be used to obtain $\mathbf{w}_\xi = \frac{\mathbf{R}^{-1}\mathbf{g}}{\mathbf{g}^T\mathbf{R}^{-1}\mathbf{g}}\xi$. Normally the covariance matrix is singular, especially when the number of samples is less than the number of EEG channels. Then the regularized inverse $\mathbf{R}^{-1} = \left(\mathbf{R} + \gamma^2\mathbf{I}\right)^{-1}$ is used instead, where $\gamma^2$ is the diagonal loading factor and $\mathbf{I}$ is the identity matrix.

By selecting different $\xi$ we can obtain different types of scalar beamformers. For S-MVB, $\xi = 1$ and the weight vector is

$$\mathbf{w}|_{\text{S-MVB}} = \frac{\mathbf{R}^{-1}\mathbf{g}}{\mathbf{g}^T\mathbf{R}^{-1}\mathbf{g}} \tag{2}$$

The S-WNMVB is derived based on the assumption that the weight vector $\mathbf{w}$ is normalized, i.e. $\mathbf{w}^T\mathbf{w} = 1$ [8]. In this case, equation (1) leads to the following expressions: $\xi^2\frac{\mathbf{g}^T\mathbf{R}^{-2}\mathbf{g}}{\left(\mathbf{g}^T\mathbf{R}^{-1}\mathbf{g}\right)^2} = 1$ and $\xi = \frac{\mathbf{g}^T\mathbf{R}^{-1}\mathbf{g}}{\sqrt{\mathbf{g}^T\mathbf{R}^{-2}\mathbf{g}}}$. Substituting $\xi$ into $\mathbf{w}_\xi$ then gives

$$\mathbf{w}|_{\text{S-WNMVB}} = \frac{\mathbf{R}^{-1}\mathbf{g}}{\sqrt{\mathbf{g}^T\mathbf{R}^{-2}\mathbf{g}}} \tag{3}$$

For S-SMVB [8], the output power is normalized such that $\mathbf{w}^T\mathbf{R}\mathbf{w} = 1$. Combining this constraint with the general formula for scalar beamformers in equation (1) gives $\xi^2\frac{1}{\mathbf{g}^T\mathbf{R}^{-1}\mathbf{g}} = 1$ and $\xi = \frac{1}{\sqrt{\mathbf{g}^T\mathbf{R}^{-1}\mathbf{g}}}$. The weight vector of S-SMVB is therefore

$$\mathbf{w}|_{\text{S-SMVB}} = \frac{\mathbf{R}^{-1}\mathbf{g}}{\sqrt{\mathbf{g}^T\mathbf{R}^{-1}\mathbf{g}}} \tag{4}$$

Using the output power of S-MVB to localize sources can lead to a biased estimation of the source locations. To reduce the localization bias, a normalized gain vector, $\frac{\mathbf{g}}{\|\mathbf{g}\|}$, is used [8].

The optimum dipole orientation $\mathbf{v}_{opt}$ is defined as the one that maximizes the output signal-to-noise ratio $J_{max} = max\left(\frac{\mathbf{v}^T\mathbf{L}^T\mathbf{R}^{-1}\mathbf{L}\mathbf{v}}{\mathbf{v}^T\mathbf{L}^T\mathbf{R}^{-2}\mathbf{L}\mathbf{v}}\right)$ [13]. The solution of the above optimization problem is actually the maximum eigenvalue $\lambda_{max}$ of the generalized eigen-decomposition: $J_{max} = \lambda_{max}\left(\mathbf{P}, \mathbf{Q}\right)$, where $\mathbf{P} = \mathbf{L}^T\mathbf{R}^{-1}\mathbf{L}$ and $\mathbf{Q} = \mathbf{L}^T\mathbf{R}^{-2}\mathbf{L}$, and the optimum orientation is the eigenvector corresponding to the maximum eigenvalue.

There is also another approach to estimate the orientation, where the normalized output power of the S-MVB is used as the optimized function: $P_{max} = max\left(\frac{\mathbf{v}^T\mathbf{L}^T\mathbf{L}\mathbf{v}}{\mathbf{v}^T\mathbf{L}^T\mathbf{R}^{-1}\mathbf{L}\mathbf{v}}\right)$. In this case, the optimum orientation $\mathbf{v}_{opt}$ is the eigenvector that corresponds to the maximum eigenvalue of the generalized eigen-decomposition of $P_{max} = \lambda_{max}\left(\mathbf{A}, \mathbf{P}\right)$, where $\mathbf{A} = \mathbf{L}^T\mathbf{L}$.

Unlike the scalar ones, the vector beamformers simultaneously reconstruct the three dipole vector components. A weight matrix is defined as $\mathbf{W}(\mathbf{r}) = [\mathbf{w}_x(\mathbf{r}), \mathbf{w}_y(\mathbf{r}), \mathbf{w}_z(\mathbf{r})]$, where $\mathbf{w}_x(\mathbf{r})$, $\mathbf{w}_y(\mathbf{r})$ and $\mathbf{w}_z(\mathbf{r})$ are weight vectors for the x, y and z directions respectively. The reconstructed dipole source is therefore $\left[\widehat{d}_x(\mathbf{r}), \widehat{d}_y(\mathbf{r}), \widehat{d}_z(\mathbf{r})\right]^T = \mathbf{W}^T(\mathbf{r})\mathbf{M}$, where $\widehat{d}_x$, $\widehat{d}_y$ and $\widehat{d}_z$ are the estimates of the dipole components in the $x$, $y$ and $z$ directions.

The vector beamformers studied before include the linearly constrained minimum variance beamformer (LCMV) and vector Borgiotti-Kaplan beamformer (V-BKB). The weight for LCMV is found by solving the optimization problem with the unity gain constraint

$$minimize \quad \left\{tr\left(\mathbf{W}^T\mathbf{R}\mathbf{W}\right)\right\} \quad \text{subject to} \quad \mathbf{L}^T\mathbf{W} = \mathbf{F} \tag{5}$$

Using again the Lagrange multiplier, $\mathbf{W}$ is obtained as [18]

$$\mathbf{W} = \mathbf{R}^{-1}\mathbf{L}\left(\mathbf{L}^T\mathbf{R}^{-1}\mathbf{L}\right)^{-1}\mathbf{F} \tag{6}$$

If $\mathbf{R}$ is singular, then the regularized inverse $\left(\mathbf{R} + \gamma^2\mathbf{I}\right)^{-1}$ is used instead. Moreover, if $\mathbf{F} = \mathbf{I}$, we then obtain the weight matrix for LCMV

$$\mathbf{W} = \mathbf{R}^{-1}\mathbf{L}\left(\mathbf{L}^T\mathbf{R}^{-1}\mathbf{L}\right)^{-1} \tag{7}$$

As mentioned in [18, 14], source localization with the output power of LCMV can also be biased towards the surface electrodes. To avoid this, the use of the normalized lead field matrix $\left[\frac{\mathbf{l}_x}{\|\mathbf{l}_x\|_2}, \frac{\mathbf{l}_y}{\|\mathbf{l}_y\|_2}, \frac{\mathbf{l}_z}{\|\mathbf{l}_z\|_2}\right]$ or the neuronal activity index was suggested, where $\|.\|_2$ is the Frobenius norm.

The constraints used for V-BKB in the minimization are [14]

$$\mathbf{w}_\xi^T\mathbf{w}_\xi = 1, \mathbf{w}_\xi^T\mathbf{g}_\eta = 0 \quad \text{with } \xi, \eta = x, y, z;\ \xi \neq \eta \tag{8}$$

where $\mathbf{g}_\eta$ is the gain vector for a dipole in the $\eta$ direction. The columns of the weight matrix can be obtained as

$$\mathbf{w}_\xi = \frac{\mathbf{R}^{-1}\mathbf{L}\mathbf{P}^{-1}\mathbf{f}_\xi}{\sqrt{\mathbf{f}_\xi^T\mathbf{H}\mathbf{f}_\xi}} \tag{9}$$

where $\mathbf{f}_\xi$ is the unit vector in the $\xi$ direction, and $\mathbf{H} = \mathbf{P}^{-1}\mathbf{Q}\mathbf{P}^{-1}$.

### 2.2. Novel vector beamformers

#### *2.2.1. Vector weight normalized minimum variance beamformer (V-WNMVB)*

It is straightforward to show that the output power of LCMV (as given in Table 2 later) has the localization bias since it depends on the Frobenius norm of the lead field matrix $\|\mathbf{L}\|_2$. To compensate for this bias, normalization of the weight matrix

**Table 1**: Scalar beamformer's metrics, where $\mathbf{R}$ is the covariance matrix, $\mathbf{g}$ is a gain vector, and $\sigma_n^2$ is the noise power for each EEG channel

| Beamformer | Output power | Output SNR |
|---|---|---|
| S-MVB | $\frac{1}{\mathbf{g}^T\mathbf{R}^{-1}\mathbf{g}}$ | $\frac{\mathbf{g}^T\mathbf{R}^{-1}\mathbf{g}}{\sigma_n^2\mathbf{g}^T\mathbf{R}^{-2}\mathbf{g}}$ |
| S-WNMVB | $\frac{\mathbf{g}^T\mathbf{R}^{-1}\mathbf{g}}{\mathbf{g}^T\mathbf{R}^{-2}\mathbf{g}}$ | $\frac{\mathbf{g}^T\mathbf{R}^{-1}\mathbf{g}}{\sigma_n^2\mathbf{g}^T\mathbf{R}^{-2}\mathbf{g}}$ |
| S-SMVB | 1 | $\frac{\mathbf{g}^T\mathbf{R}^{-1}\mathbf{g}}{\sigma_n^2\mathbf{g}^T\mathbf{R}^{-2}\mathbf{g}}$ |

was proposed in [3]. This gives the so-called vector weight normalized minimum variance beamformer (V-WNMVB) with

$$\mathbf{W} = \mathbf{R}^{-1}\mathbf{L}\mathbf{P}^{-1}\left(\mathbf{P}^{-1}\mathbf{Q}\mathbf{P}^{-1}\right)^{-\frac{1}{2}} \tag{10}$$

The detail derivation of the V-WNMVB is shown in [4] and the expressions for its metrics are shown in Table 2.

#### 2.2.2. *Vector standardized minimum variance beamformer (V-SMVB)*

Similar to the V-WNMVB, localization bias in identifying deep brain sources can be compensated by normalizing the output power of the LCMV beamformer. For this type of beamformer we select $\mathbf{F}$ such that the output power is normalized, so $\mathbf{W}^T\mathbf{R}\mathbf{W} = \mathbf{I}$ and the weight matrix is given by

$$\mathbf{W} = \mathbf{R}^{-1}\mathbf{L}\mathbf{P}^{-\frac{1}{2}} \tag{11}$$

All metric expressions for V-SMVB are also given in Table 2, and their detailed derivations are shown in [4].

#### 2.2.3. *Metrics*

The dipolar localization error (DLE), defined as the distance between the original and estimated dipole locations, is probably the most basic quantity for evaluating beamformer's performance. Other quantities used in our analysis and comparison include the following: 1) the full width at half maximum (FWHM); 2) the reconstructed source signal. The final expressions for the output power and output SNR of all beamformers are shown in Tables 1 and 2. An efficient way for computing these two quantities will be described below.

#### 2.2.4. *An efficient algorithm to compute the output power/SNR of SAM, V-WNMVB, and V-SMVB*

Let $\mathbf{X} = \mathbf{U}\mathbf{S}\mathbf{V}^T$ be the singular eigen-decomposition of $\mathbf{X} = \mathbf{R}^{-1}\mathbf{L}$. Then we can rewrite the generalized eigenvalues of $\mathbf{P}$ and $\mathbf{Q}$ as $\lambda(\mathbf{P},\mathbf{Q}) = \lambda\left(\mathbf{X}^T\mathbf{R}\mathbf{X},\mathbf{X}^T\mathbf{X}\right) = \lambda\left(\mathbf{V}\mathbf{S}\mathbf{U}^T\mathbf{R}\mathbf{U}\mathbf{S}\mathbf{V}^T,\mathbf{V}\mathbf{S}^2\mathbf{V}^T\right)$ or $\lambda(\mathbf{P},\mathbf{Q}) = \lambda\left(\mathbf{U}^T\mathbf{R}\mathbf{U}\right)$ [7]. Hence, the generalized eigen-decomposition is converted to a symmetric eigen-decomposition problem, which improves the numerical stability of the output power/SNR calculation when the lead field matrix $\mathbf{L}$ or $\mathbf{Q} = \mathbf{L}^T\mathbf{R}^{-2}\mathbf{L}$ is not full rank. An efficient way to compute the output SNR for SAM is given in Algorithm 1. It is straightforward to show that similar algorithms can be used to compute the output power/SNR of V-WNMVB and V-SMVB.

**Table 2**: Vector beamformer's metrics, where $\mathbf{P} = \mathbf{L}^T\mathbf{R}^{-1}\mathbf{L}$, $\mathbf{Q} = \mathbf{L}^T\mathbf{R}^{-2}\mathbf{L}$, $\mathbf{H} = \mathbf{P}^{-1}\mathbf{Q}\mathbf{P}^{-1}$, and $K$ is the number of sources

| Beamformer | Output power | Output SNR |
|---|---|---|
| LCMV | $tr\left(\mathbf{P}^{-1}\right)$ | $\frac{tr\left(\mathbf{P}^{-1}\right)}{\sigma_n^2 tr\left(\mathbf{H}\right)}$ |
| V-BKB | $\sum_{\xi=x,y,z}\frac{\mathbf{f}_\xi^T\mathbf{P}^{-1}\mathbf{f}_\xi}{\mathbf{f}_\xi^T\mathbf{H}\mathbf{f}_\xi}$ | $\frac{\sum_{\xi=x,y,z}\frac{\mathbf{f}_\xi^T\mathbf{P}^{-1}\mathbf{f}_\xi}{\mathbf{f}_\xi^T\mathbf{H}\mathbf{f}_\xi}}{3\sigma_n^2}$ |
| V-WNMVB | $tr\left(\mathbf{P}\mathbf{Q}^{-1}\right)$ | $\frac{tr\left(\mathbf{P}\mathbf{Q}^{-1}\right)}{3K\sigma_n^2}$ |
| V-SMVB | $3K$ | $\frac{3K}{\sigma_n^2 tr\left(\mathbf{Q}\mathbf{P}^{-1}\right)}$ |

**Algorithm 1** An efficient algorithm for computing the output SNR of SAM

1: **for** each node inside the brain region **do**
2: Compute the lead field matrix $\mathbf{L}$ for the current node and a left singular vector $\mathbf{U}$ of $\mathbf{L}$, where $\mathbf{L} = \mathbf{U}\mathbf{S}\mathbf{V}^T$.
3: $SNR_{out} = \lambda_{max}\left(\mathbf{U}^T\mathbf{R}\mathbf{U}\right)$
4: **end for**

## 3. NUMERICAL STUDIES

In the numerical studies, we use a $176 \times 240 \times 256$ realistic head model with a resolution of $1\,mm \times 1\,mm \times 1\,mm$ and constructed from an T1-weighted MRI image. The forward problem is solved with our finite difference neuroelectromagnetic modeling software (FNS) [5]. The MRI image is segmented using the FMRIB Software Library (FSL) [16, 17, 10, 19] to get the white matter, gray matter, cerebro-spinal fluid, skull and skin tissues. Two eye balls are segmented manually using ITKSNAP [20]. The final segmented head model is built from all the resulting masks using FNS utilities [5]. Our realistic head model has 6 tissues with the following conductivities (S/m): white matter–0.14; gray matter–0.33; cerebro-spinal fluid–1.79; skull–0.018; scalp–0.44; eyes–1.79 [11, 12].

### 3.1. Monte-Carlo simulation studies

In this simulation study, 1358 dipole locations, which span the whole gray matter region, are selected using the constraint logic programming technique (CLP) with the minimum distance constraint between any two dipole locations being

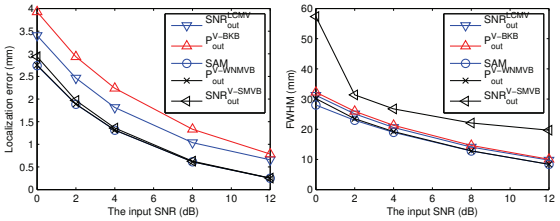


**Fig. 1**: Fixed source simulation results

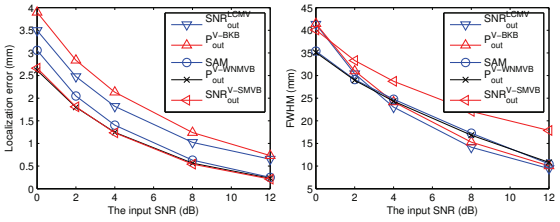


**Fig. 2**: Rotated source simulation results

$d_{min} = 10\ mm$. We generate the EEG signals for each dipole after selecting randomly one orientation $\mathbf{v}$ from 33 dipole orientations distributed uniformly over the unit sphere with the angle constraint $\theta_{max} = 30^o$, where $\theta_{max}$ is defined as the maximum angle between any two orientations. The simulated brain sources are sinusoidal signals with amplitude $1\,\mu$A and its frequency is selected randomly from 5 to 100 Hz. We use 5 values of input SNR: 0, 2, 4, 8 and 12 dB. For each dipole, we generate 50 trials of white noise with different seeds. Finally, we collect dipole localization error (DLE) and full width at half maximum (FWHM) data for 338500 cases, and the average values are reported.

Figure 1 shows the DLE and FWHM of the different beamformers, where $P_{out}$ and $SNR_{out}$ stand for the output power and output SNR, respectively. Here, we can easily see that the DLEs of V-WNMVB and V-SMVB are very close to that of SAM, even though they do not require any assumption about the dipole orientation. Moreover, our Monte-Carlo simulation studies also show that the output SNR or neural activity index of LCMV has a higher localization accuracy than that of V-BKB. This finding is new and gives a more complete view of the performance of LCMV and V-BKB.

In the rotated source simulations, each dipole's orientation can fluctuate around the orientations used in the fixed dipole simulation, and the maximum agular fluctuation is $30^0$. The simulation results are shown in Figure 2. They show that both V-WNMVB and V-SMVB have higher localization accuracy than SAM, LCMV and V-BKB. Moreover, the FWHM of SAM and V-WNMVB are very similar and that of V-SMVB is the worst for a moderate to high input SNR.

### 3.2. Multiple source simulation studies

In this study we simulate 3 brain sources to imitate the physiological distribution of spontaneous brain activities. These

**Table 3**: Dipole localization errors (mm)

| Beamformer | 1st source | 2nd source | 3rd source |
|---|---|---|---|
| LCMV | 6.08 | 2.45 | 1.73 |
| V-VKB | 6 | 7.35 | 4.12 |
| SAM | 2.45 | 1 | 1.73 |
| V-WNMVB | 2.45 | 1 | 1.73 |
| V-SMVB | 2 | 1.41 | 1.41 |

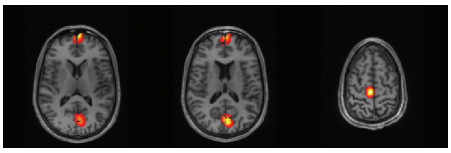

**Fig. 3**: Transverse cross-sectional views of tomographic map for SAM

3 sources are located at frontal cortex, parieto-occipital sulcus and sensorimotor hand area with the amplitude of 3 $\mu$A, 5 $\mu$A, and 1 $\mu$A and frequency of 22 Hz, 15 Hz, and 8 Hz, respectively. To make the simulation more realistic, we add Gaussian white noise with an input SNR $= 2$ dB. Once the EEG signals are generated, we use LCMV, V-BKB, SAM, V-WNMVB, and V-SMVB to localize and reconstruct all sources. The dipole localization errors for each beamfomer are shown in Table 3. We can easily verify that the DLEs of both V-WNMVB and V-SMVB are as good as those of SAM. Figures 3 and 4 show 3 different transverse cross-sectional views of the tomographic maps for SAM and V-WNMVB, which are similar and very focal. The output tomographic map of V-SMVB, as shown in Figure 5, however, is wide spread.

## 4. CONCLUSIONS

Two new vector beamformers, namely V-WNMVB and V-SMVB, have been devloped and tested. They show better localization accuracy than conventional beamformers, including LCMV and V-BKB, in both single (fixed and rotated) and multiple source studies. These beamformers are promisng for real applications where a vector beamformer is desired. Moreover, these new beamformers can be combined with Dynamic Imaging of Coherent Sources to localize the brain sources in the frequency domain.

New efficient algorithms for computing the output SNR of SAM, the output power of V-WNMVB and the output SNR

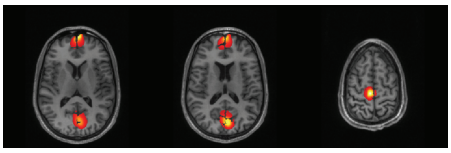

**Fig. 4**: Transverse cross-sectional views of tomographic map for V-WNMVB

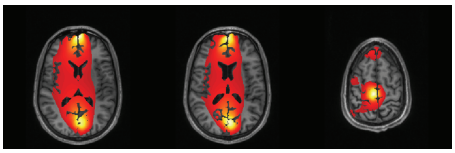

**Fig. 5**: Transverse cross-sectional views of tomographic map for V-SMVB

of V-SMVB are proposed. These algorithms help reduce the numerical error when the lead field matrix is not full rank.

## 5. REFERENCES


[1] S. Baillet, J. C. Mosher, and R. M Leahy. Electromagnetic brain mapping. *Signal Processing Magazine, IEEE*, 18(6):14–30, Nov 2001.

[2] S.S. Dalal, K. Sekihara, and S.S. Nagarajan. Modified beamformers for coherent source region suppression. *IEEE Trans. Biomed. Eng.*, 53(7):1357 –1363, July 2006.

[3] Hung V. Dang. Performance analysis of EEG adaptive beamformers. Master's thesis, New Mexico State University, 2007.

[4] Hung V. Dang. *Novel beamgorming algorithms for EEG source imaging applications*. PhD thesis, New Mexico State University, 2010.

[5] Hung V. Dang and Kwong T. Ng. Finite difference neuroelectromagnetic modeling software. *In review*, 2010.

[6] Mithun Diwakar, Ming-Xiong Huang, Ramesh Srinivasan, Deborah L. Harrington, Ashley Robb, Annemarie Angeles, Laura Muzzatti, Reza Pakdaman, Tao Song, Rebecca J. Theilmann, and Roland R. Lee. Dual-core beamformer for obtaining highly correlated neuronal networks in MEG. *NeuroImage*, In Press, Corrected Proof:–, 2010.

[7] Gene H. Golub and Charles F. Van Loan. *Matrix Computation (Johns Hopkins Studies in Mathematical Sciences)*. The Johns Hopkins University Press, 3rd edition, 1996.

[8] R.E. Greenblatt, A. Ossadtchi, and M.E. Pflieger. Local linear estimators for the bioelectromagnetic inverse problem. *IEEE Trans. Biomed. Eng.*, 53(9):3403–3412, Sept. 2005.

[9] J. Gross, J. Kujala, M. Hamalainen, L. Timmermann, A. Schnitzler, and R. Salmelin. Dynamic imaging of coherent sources: Studying neural interactions in the human brain. *PNAS*, 98(2):694–699, January 2001.

[10] M. Jenkinson, M. Pechaud, and S. Smith. Bet2: Mr-based estimation of brain, skull and scalp surfaces. Eleventh Annual Meeting of the Organization for Human Brain Mapping, 2005.

[11] C. Ramon, P. Schimpf, J. Haueisen, M. Holmes, and A. Ishimaru. Role of soft bone, csf and gray matter in EEG simulations. *Brain Topogr.*, 16:245–248(4), 2004.

[12] C. Ramon, P. H. Schimpf, and J. Haueisen. Influence of head models on EEG simulations and inverse source localizations. *BioMedical Engineering Online*, 5, February 2006.

[13] S. E. Robinson and J. Vrba. Functional neuroimaging by synthetic aperture magnetometry (SAM). *Recent Advances in Biomagnetism*, pages 302–305, 1999.

[14] K. Sekihara, S.S. Nagarajan, D. Poeppel, A. Marantz, and Y. Miyashita. Reconstructing spatio-temporal activities of neural sources using an MEG vector beamformer technique. *IEEE Trans. Biomed. Eng.*, 48:760–771, 2001.

[15] K. Sekihara, S.S. Nagarajan, D. Poeppel, A. Marantz, and Y. Miyashita. Performance of an MEG adaptive-beamformer technique in the presence of correlated neural activities: effects on signal intensity and time-course estimates. *IEEE Trans. Biomed. Eng.*, 49:1534–1546, 2002.

[16] S.M. Smith. Fast robust automated brain extraction. *Hum. Brain Mapp.*, 17(3):143–155, November 2002.

[17] S.M. Smith, M. Jenkinson, M.W. Woolrich, C.F. Beckmann, T.E.J. Behrens, H. Johansen-Berg, P.R. Bannister, M. De Luca, I. Drobnjak, D.E. Flitney, R. Niazy, J. Saunders, J. Vickers, Y. Zhang, N. De Stefano, J.M. Brady, and P.M. Matthews. Advances in functional and structural MR image analysis and implementation as FSL. *Neuroimage*, 23(1):208–219, 2004.

[18] B. D. Van Veen, W. Van Drongelen, M. Yuchtman, and A. Suzuki. Localization of brain electrical activity via linearly constrained minimum variance spatial filtering. *IEEE Trans. Biomed. Eng.*, 44:867–880, 1997.

[19] M.W. Woolrich, S. Jbabdi, B. Patenaude, M. Chappell, S. Makni, T. Behrens, C. Beckmann, M. Jenkinson, and S.M. Smith. Bayesian analysis of neuroimaging data in fsl. *NeuroImage*, 45:S173–S186, March 2009.

[20] Paul A. Yushkevich, Joseph Piven, Heather Cody Hazlett, Rachel Gimpel Smith, Sean Ho, James C. Gee, and Guido Gerig. User-guided 3D active contour segmentation of anatomical structures: Significantly improved efficiency and reliability. *Neuroimage*, 31(3):1116–1128, 2006.